

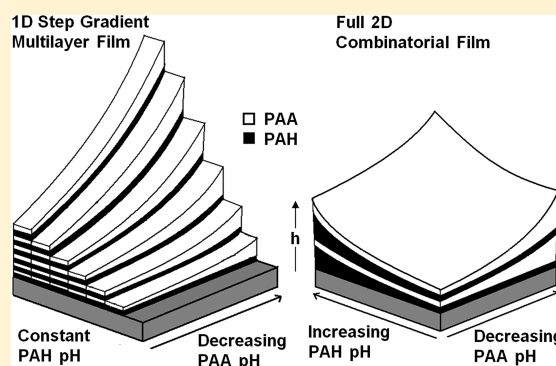
Fabrication of Two-Dimensional Gradient Layer-by-Layer Films for Combinatorial Biosurface Studies

Miloslav Sailer and Christopher J. Barrett*

Department of Chemistry, McGill University, Montreal, Quebec H3A 0B8, Canada

ABSTRACT: We have developed a novel gradient fabrication method for combinatorial surface studies that provides the equivalent of 5000 individual polyelectrolyte multilayer (PEM) film physicochemical conditions in a single 7 cm square film. A simple, inexpensive, and versatile automated layering instrument was built, which can generate a gradient of physical properties on a film in 1 dimension laterally by simultaneously changing both the location of polyelectrolyte adsorption and the layering conditions, such as pH or salt concentration of the polyelectrolyte dipping solutions. By rotating the substrate 90° after each deposition cycle, full 2-dimensional gradient combinatorial films were fabricated over many layers, spanning virtually all previous combinations of stable deposition pH and salt conditions for both poly(allylamine hydrochloride) (PAH) and poly(acrylic acid) (PAA), a process which previously required more than 10 000 separate film samples.

Surface spatial profiles of film thickness, surface energy (wettability), density (refractive index), and stiffness (modulus) were generated and correlated to assembly conditions. Additionally, step gradient films were generated first by varying the number of bilayers along one axis and pH along the other, which enabled us to measure their combined effect on thickness. To test for biocompatibility, we incubated HEK 293 cells on step gradient films and 2D combinatorial films for 48 h and determined that film assembly conditions played a major role, especially in controlling the stiffness and the density, which could be tailored with deposition pH over a wide range. Optimal growth conditions were discovered not at the extremes of fabrication pH, but instead near PAH pHs of 4–6 and PAA pH around 4, demonstrating that these PEM biosurfaces and this technique are suitable for optimizing high-throughput cellular screening.



INTRODUCTION

Polyelectrolytes that spontaneously self-assemble on oppositely charged surfaces to form stable, electrostatically bound monolayers have been well studied. Upon adsorption, excess segments of polyelectrolyte chains get exposed on the surface, overcompensating for and reversing their charge. If the coated surface is then immersed in a solution of the oppositely charged polyelectrolyte, a stable bilayer will form that reverts the surface back to its original charge, resetting it for the adsorption of another layer. This coating process to build thin films, called layer-by-layer (l-b-l) assembly, is now a well established technique for preparing polyelectrolyte multilayers (PEMs) from aqueous media^{1,2} and is especially appealing for soft, wet, charged coatings for a wide variety of “bio” applications. PEMs have found their way into various precision application areas such as optical coatings,³ macromolecular encapsulation,^{4,5} and biocompatible coatings for artificial implant materials, dubbed “biocomoflage”.⁶ For such applications, optimization of the physical properties of PEMs is crucial; it was discovered by Decher in the earliest stages of PEM development¹ that it was possible to tune these properties by altering the charge density of the polyelectrolytes during deposition. Accordingly, some of the most interesting PEMs are now built from weak polyelectrolytes, as they have charge fractions that are influenced by pH, unlike strong polyelectrolytes, leading to easily tailorable properties over a wide range.

The two most well-studied weak polyelectrolytes used in PEM fabrication are perhaps poly(acrylic acid) (PAA) and poly(allylamine hydrochloride) (PAH) (Figure 1), which both

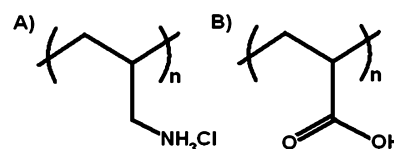


Figure 1. Molecular structures of (A) poly(allylamine hydrochloride) and (B) poly(acrylic acid).

have charge fractions that are strongly sensitive to pH.⁷ This strong sensitivity means that varying the pH range from weakly charged to strongly charged for both the polycations and polyanions results in many thousands of different pH combinations leading to distinguishable end properties; thus, many thousands of effectively different films can be made from just the same two polyelectrolytes. Fabricating, characterizing, and testing this vast number of separate films are thus expensive, time-consuming, prone to irreproducibility, and thus

Received: March 28, 2012

Revised: June 19, 2012

Published: June 29, 2012

effectively unrealistic as a research strategy. The field of combinatorial materials science however has recently emerged to provide powerful tools to deal with such complex materials systems: systems that contain a considerable and complex parameter space are highly tailored (i.e., composition, structure, and properties are optimized for a specific application), are formulated from a number of components sensitive to processing routes, and exhibit intricate structure and behavior.⁸ Combinatorial methods have been used to develop materials such as biodegradable polymers,⁹ polymeric supports for organic synthesis,¹⁰ sensors for herbicides,¹¹ and biocompatible materials.^{12,13}

However, despite being a highly tailored and formulated material with an intricate structure and behavior, PEMs have not yet to our knowledge been prepared and investigated through combinatorial means. Accordingly, this paper proposes a new combinatorial method for the fabrication of PEM films. The method works by slowly and continuously filling up a changing deposition bath as the sample is held vertically, altering the effective charge density of PAH along the y -axis during the layering process, then rotating the sample 90° and repeating this process with PAA along the x -axis, again pumping in a gradient of solution conditions as the bath slowly fills up, leading to a second “vertical” gradient, now orthogonal to the first (Figure 2). Similar dipping techniques

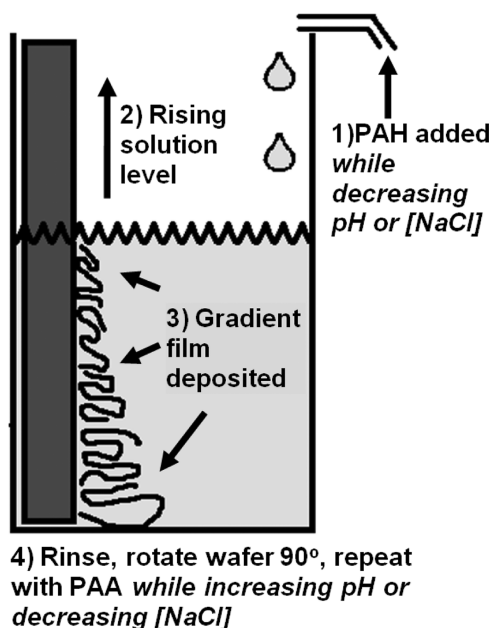


Figure 2. Schematic of the 2D gradient film fabrication process.

have been used by Tomlinson and co-workers^{14,15} where they made polymer brushes by either slowly draining or increasing the level of solution with time-dependent polymer growth. Xu and co-workers¹⁶ also used gradient dipping to alter the % composition of a MMA/HEMA monomer mixture during polymerization, while the level of solution increased.

Using our technique, the result is a single 2D combinatorial gradient film containing all pH combinations: the equivalent of many thousands of different possible films (Figure 3A). One estimate of how many films are represented combinatorially is to compare the distance along each axis that separate measurements could be made beyond error bars, which for our $7\text{ cm} \times 7\text{ cm}$ films was about 1 mm each, for a total of $70 \times$

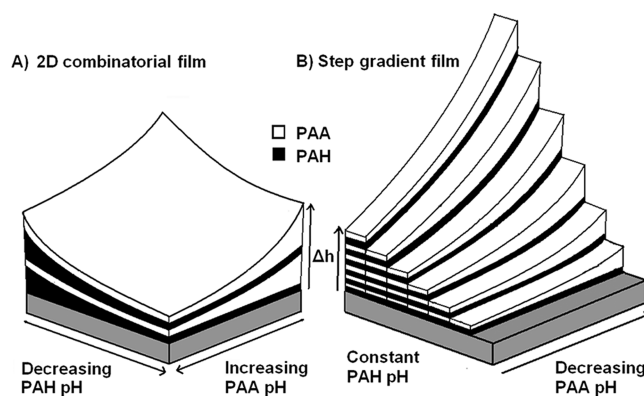


Figure 3. Proposed rationale for (A) 2D combinatorial PEM and (B) step gradient films.

70 distinct and unique measurement per film. Larger surfaces or more precise measurements could easily generate 100 000 distinct locations by this new method. Surface maps of thickness, refractive index, and surface energy were then generated and directly correlated to fabrication conditions. Additionally, films containing up to six individual bilayers were generated by varying the pH of one polyelectrolyte solution on the y -axis and the number of bilayers on the x -axis (Figure 3B). These step gradient and combinatorial films were used to investigate HEK 293 cell viability, to assess the general suitability of the gradient films to study a variety of biosurface applications.

EXPERIMENTAL METHODS

Sample Preparation. PAA (MW 100 000, Sigma-Aldrich), stock solutions were made by diluting an aqueous 35% PAA solution with deionized water (Milli-Q, $18.2\text{ M}\Omega/\text{cm}$) to 0.01 M; a PAH (MW 65 000, Sigma-Aldrich) stock solution of 0.01 M was made by dissolving solid PAH-HCl in deionized water. The pH of stock solutions was adjusted using 1 M NaOH and 1 M HCl. Silicon wafers (S44748 4N EPI PRIME SB (100), $500\ \mu\text{m}$, WaferNet) were underscored using a diamond knife and cleaved into $7 \times 7\text{ cm}$ square wafers that were then cleaned by immersion in a “piranha” cleaning bath (3:1 concentrated sulfuric acid: 30% hydrogen peroxide; *caution: piranha is a strong oxidizer and should not be stored in closed containers*) and heated for 30 min. The cleaned wafers were then rinsed vigorously for 20 min with deionized water and preserved under WF-30-X0 gel films (Gel-Pak) until use.

Calibration of Layering Device. Before film deposition, it was necessary to measure how the pH of the solution pumped in changed with time and thus “vertical” position on the subsequent films. 200 mL of the PAH (pH 11) stock solution was pumped (mini-pump variable flow, Fisher) into a glass container slightly larger than the wafer, while a 0.4 M HCl solution was pumped into the stock PAH solution to a total of $<10\text{ mL}$ to avoid significant dilution. The pH change in the glass container was measured by a pH meter (Orion Model 420A) interfaced with a computer, and the pH readings were recorded using Hyperterminal (Private edition v 5.0) every 5 s until the container was filled. This process was repeated for the PAA (pH 3) stock solution with a 0.4 M NaOH solution (Figure 4). The whole filling process covered the vertical rise of 7 cm in $\sim 50\text{ min}$.

Assembly of 2D Gradient pH Films. The silicon wafers were placed in the empty deposition bath, while the solution of PAH with varying pH (Figure 4) was added slowly while stirring. The resultant film was then rinsed, rotated by 90° , and placed in the empty bath container that then started filling again, to gradually immerse the film in a solution of PAA with varying pH (Figure 4) while stirring, for a second vertical gradient, now orthogonal to the first. The film was

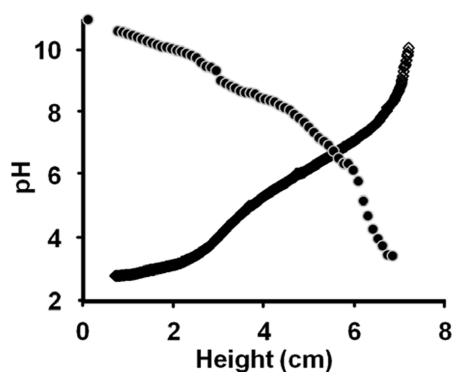


Figure 4. Calibration curves for PAH using 0.4 M HCl (●) and PAA using 0.4 M NaOH (◇).

rinsed and the entire process was repeated until 10 layers were deposited.

Assembly of 2D Gradient Salt Films. Similarly to changing pH, the [ion] could also be introduced slowly. Initially, the pH of PAA and PAH was set to 4.5 and 8.5, respectively. PAH was then pumped into a glass container with 2 mL of 0.25 g/mL NaCl starter solution while stirring, until the container was filled. The wafer was then rinsed and rotated by 90°, and a layer PAA was deposited in the same way. The process was repeated until 10 layers were deposited.

Assembly of Step Gradient Films. Strips of WF-30-X0 gel films to act as protective covers were cut into 6.1 × 7 cm rectangles and placed over the cleaned silicon wafers, leaving one just exposed strip of silicon initially. The partially masked silicon surface was immersed in a solution of PAH at varying pH (pH 11–3) while stirring, followed by a rinse with Milli-Q water and complete immersion into a solution of PAA at a constant pH for 10 min. Following another rinse, a second gel strip adjacent to the first was removed, and the whole process was repeated until six bilayers were obtained, revealing adjacent strips to produce $n - 1$ layers each of n steps. The last gel strip was removed after all layering was complete as a blank reference of zero layers. This entire layering process was carried out using different PAA solutions with fixed pHs (3, 4.5, and 10). The process was then repeated while keeping the pH of the PAH solution fixed (3, 8.5, and 11) and varying the pH of the PAA solution (3–10). The spacing of pH increments was decreased in regimes of strong thickness sensitivity by decreasing the polyelectrolyte solution flow rate.

Thickness Measurements. The thicknesses of the gradient multilayer films were measured using single wavelength (633 nm) null-ellipsometry (Optrel, Multiskop) fixed at 70° to the normal. The films were allowed to equilibrate with lab atmospheric humidity conditions 16 h overnight before measurements were taken. Films were placed on a moveable stage (Δ 1 mm) with individual measurements of Δ and ψ being taken at intervals of between 1 and 5 mm. Measurements of Δ and ψ were then processed using an appropriate model (air ($n = 1.00$)/film ($t = x$, $n = x$)/SiO₂ ($t = 2.3$ nm, $n = 1.54$)/Si ($n = 3.42$, $k = -0.011$)) to obtain thickness and refractive index values.

Cell Viability Assays. Human embryonic kidney 293 (HEK 293) cells were cultured in Dulbecco's modified Eagle medium (DMEM, Invitrogen) supplemented with 100 unit/mL penicillin G (Invitrogen), 100 μ g/mL streptomycin (Invitrogen), and 10% fetal bovine serum (Invitrogen). Cultured cells were incubated in a 5% CO₂ and 37 °C humidified incubator. For viability assays, 15 000 HEK 293 cells/cm² were plated on each PEM film coated silicon wafer. Following one day growth in vitro (DIV), HEK 293 cells were fixed with 4% paraformaldehyde (PFA, Fisher Scientific) and 0.1% glutaraldehyde (Sigma) for 60 s and then blocked with 3% horse serum (HS, Invitrogen) and 0.1% Triton X-100 (Fisher Scientific). Cells were stained with 0.8 unit/mL Alexa 488-coupled Phalloidin and 500 ng/mL Hoechst 33258. Films were coverslipped using FluoroGel (Electron Microscopy Sciences).

Cell Imaging and Counting. Cells were imaged using an Axiovert 100 inverted fluorescence microscope (Carl Zeiss Canada, Toronto, ON) with a Magnafire CCD camera and MagnaFire 4.1C imaging software (Optronics, Goleta, CA). Images were captured at positions equivalent to thickness measurement locations (controlled by an x - y Δ 1 mm stage). The number of cells was quantified by counting Hoechst positive nuclei using ImageJ software (U.S. National Institutes of Health, Bethesda, MD). The macro used for cell counting consisted of conversion to a 16-bit picture format, background subtraction, threshold adjustment to exclude background, conversion to binary, and a cell count. The same macro was used for all images to ensure consistent counts. 2D "phase plots" of relative cell viability were generated through total cell counts of nuclei after 48 h incubation for each of 196 images spaced uniformly every 5 mm across each axis (14 × 14 images) on the entire 7 × 7 cm wafer.

Modulus Measurements Using Atomic Force Microscopy (AFM). Force measurements of the multilayer films were performed using an AFM in force calibration mode (Nanoscope Version 3A, Digital Instruments), similar to previously published methods and analysis.¹⁷ The multilayer surface and the tip were brought together in a fluid cell at room temperature. Silicon nitride probes were used (radius = 20–60 nm) with a manufacturer specified force constant, k , of 0.12 N/m. All modulus measurements of the films were performed with the same AFM tip: no calibration for the absolute spring constant of the tip was performed. The AFM detector sensitivity was calibrated by obtaining a force curve on a bare substrate and determining the slope of the linear portion of the data after contact. Obtaining force curves of the multilayer film involved bringing the tip in close contact with the surface in aqueous media and obtaining force measurements after allowing the system to equilibrate for 10 min or until reproducible curves were observed. The rate of the indentation cycle was kept constant at 0.2 Hz. For modulus measurements, four replicate measurements of the tip deflection as a function of the piezo z -position were acquired with the unmodified AFM tip, and the curves were converted into modulus as described previously.¹⁷

Surface Energy Measurements. Surface energy was approximated by a contact angle measurement performed using the sessile drop technique by depositing ~ 3 μ L of Milli-Q pure water and diiodomethane (CH₂I₂) on the surface of the films. An EHDkam-Pro02 high-resolution digital camera mounted on a moveable stage was used to acquire images of the droplets that were then analyzed with the Young–Dupree model. Contact angle measurements were converted to surface energies using the Fowkes approach,¹⁸ and all images were taken on the same day to reduce error from fluctuation in air humidity (10%).

RESULTS AND DISCUSSION

Instrument Design. In order to generate gradient combinatorial films, we designed and built a simple, inexpensive, and versatile automated layering instrument. Our aim was to simultaneously change both the pH of the polyelectrolyte solution and the vertical location of polyelectrolyte adsorption. This was achieved by using two variable flow pumps and three containers as (1) the acid or base reservoir, (2) the polyelectrolyte solution reservoir at a preset pH, and (3) the silicon wafer deposition bath for assembly. By pumping the acid or base slowly into the polyelectrolyte solution, the pH was slowly altered at each height as it filled from empty to full; this solution of slowly changing pH was concurrently pumped into the container with the silicon wafer. Through the correlation of the pH change to the height of the solution in the layering chamber containing the silicon wafer, the vertical location of polyelectrolyte adsorption conditions at a specific pH could be determined. Using this instrument, by modifying initial pHs, flow rates, and molarities, enables the fabrication of a wide range of gradient films, such as a film that has a deposition pH range of 11–3 with measurable increments of

0.1 pH units or one that has a deposition pH range of 8–10 with measurable increments of 0.01 pH units. This layering technique is however only suitable for systems where layer adsorption is irreversible, as the previously adsorbed polyelectrolyte is exposed to the changing solution conditions during the slow dipping process, and the assumption is that once adsorbed under conditions of a certain pH or [ion], this structure is “locked in” and will not change even when the entire deposition solution changes pH or [ion] to deposit different layer properties at a later time at higher vertical rise. Therefore, the layer properties are determined at the moment of adsorption and are immune to significant reorganization under different solution conditions.¹⁹ To assist this assumption, in order for the calibration (Figure 4) to be consistent with resultant pH at adsorption level vertically, the time scale for the polyelectrolytes to adsorb onto the surface and “lock” their conditions must be faster than the solution increase in height. Previous work done in our group suggests that maximal adsorption of polyelectrolytes at the concentration used in these experiments are within a few seconds (1–10) of dipping.²⁰ Therefore, the flow rate was set so that the lateral increase in volume was relatively slow: equal to or less than 230 $\mu\text{m/s}$ and so on the same scale with which the films are characterized ($\Delta 1 \text{ mm}$): adsorption pH is accurately correlated to the calibration curve.

In this study three kinds of gradients were designed to approximate many thousands of separate film conditions: (a) a full 2-dimensional gradient film spanning all usual previous pH fabrication conditions, (b) a 2-dimensional gradient film spanning all usual previous salt concentrations, and (c) a bilayer series of linear step gradients spanning hundreds of deposition pH combinations over several bilayers to test the effect of the number of layers.

a. 2D Combinatorial Gradient Films Varying pH. Figure 5A shows the thickness map of a (PAA/PAH)₅ PEM film

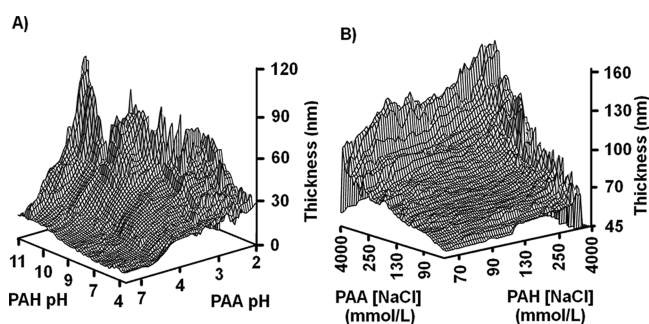


Figure 5. A thickness map of a (PAA/PAH)₅ PEM films generated from (A) grayscale pH assembly combinations and (B) a grayscale salt concentration assembly combination. Missing data points reflect the instability of the film under certain conditions that lead to cloudiness that precluded reliable ellipsometry.

fabricated by varying the deposition pH of PAA from 2.5 to 10 across the x -axis and varying the deposition pH of PAH from 11 to 3 on the y -axis. The thickness profile illustrates the high sensitivity of thickness to assembly pH, the nature of which has always been observed to be complex and is still not fully understood. Past research^{7,21,22} suggests that through an ion exchange process polyelectrolytes substitute counterions from the surface (i.e., $-\text{NH}_3^+\text{Cl}^- \rightarrow -\text{NH}_3^+\text{COO}^-$) and intrinsically compensate for the surface charge to form an electrostatic link with the surface. This often traps segments of polyelectrolytes

into loops ($-\text{NH}_3^+-\text{OOC}-\text{X}-\text{COO}-^+\text{H}_3\text{N}-$) and tails ($-\text{NH}_3^+-\text{OOC}-\text{X}$) of X-mers that protrude from the surface and remain extrinsically charge-compensated ($-\text{COO}^-\text{Na}^+$). The length of the loops and tails formed increases with decreasing charge ratio of the polyelectrolytes ($-\text{COOH}/-\text{COO}^-$ or $-\text{NH}_2/-\text{NH}_3^+$) due to the adoption of a globular structure in solution and a corresponding decrease in frequency of intrinsic charge compensation. Furthermore, at a reduced charge ratio, polyelectrolyte diffusion into the PEM is increased due to the reduction of the electrostatic barrier formed at the solution/PEM interface. Rinsing traps these polyelectrolytes inside of the PEM, and so upon subsequent dipping they become attracted to the incoming oppositely charged polyelectrolytes and form electrostatic links with them, increasing the amount of polyelectrolytes in the previous layer and thus the thickness.²¹ Generally, the lower the charge ratio at which PEMs are made, the thicker the films formed will be (Figure 5A). At extremely low charge ratios the PEM film was found to be unstable, likely due to inadequate electrostatic cross-link formation.

b. 2D Combinatorial Gradient Films Varying [Ion]. A 2D gradient film was prepared similarly by fixing the pH of PAA and PAH to 4.5 and 8.5, respectively, but then varying the salt concentration from >4 to $<0.05 \text{ M}$ by dilution (Figure 5B). This was accomplished by starting with a small amount of highly concentrated starter solution placed just below the bottom of the wafer, then adding the unsalted polyelectrolyte solution, to continuously dilute from 4 M to a final [ion] of 0.05 M, as the volume increased by 2 orders of magnitude. The thickness profiles of these resultant films suggest that an increase in ion concentration increases thickness directly and independently of polyelectrolyte used. As well as making the polyelectrolyte more globular, a higher salt concentration reduces the frequency of cross-link formation since polyelectrolyte adsorption is primarily a competitive ion exchange process. This results in longer loops and tails and thus increased thickness of the PEM films. Moreover, at high salt concentration the Debye length is reduced, reducing the electrostatic barrier and increasing diffusion of polyelectrolytes into the PEM, leading to thicker films. At extreme salt concentrations ($>4 \text{ M}$), no film is assembled on the surface due to massive charge shielding and lack of intrinsic charge compensation.

Since a region containing an unstable pH combination was discovered that lead to cloudy films unsuitable for optical analysis (Figure 5A), second generation films were fabricated using only stable PAA/PAH pH combinations (Figure 6). Comparing thickness and refractive index profiles of these films, it was observed that the thickness of the film was inversely correlated with the refractive index, which ranged from 1.53 to 1.81 (Figure 6B). Within an optically transparent system, a change in the refractive index provides a good approximation for change in the density of the film and when coupled with thickness measurements provides information about the internal architecture.²³ In the thickest regions of the film (i.e., at PAH pH ~ 10.5 , PAA pH ~ 3.5) the lowest refractive index is observed (~ 1.53). This confirms that the increase in thickness is not solely due to an increase in the amount of polyelectrolyte adsorbed but that at those assembly pH conditions the conformation of the polyelectrolytes is such that a lower density film is obtained. Finally, one must realize that the disproportionately large refractive indices observed at the thinnest areas of the film could be artifacts due to the large

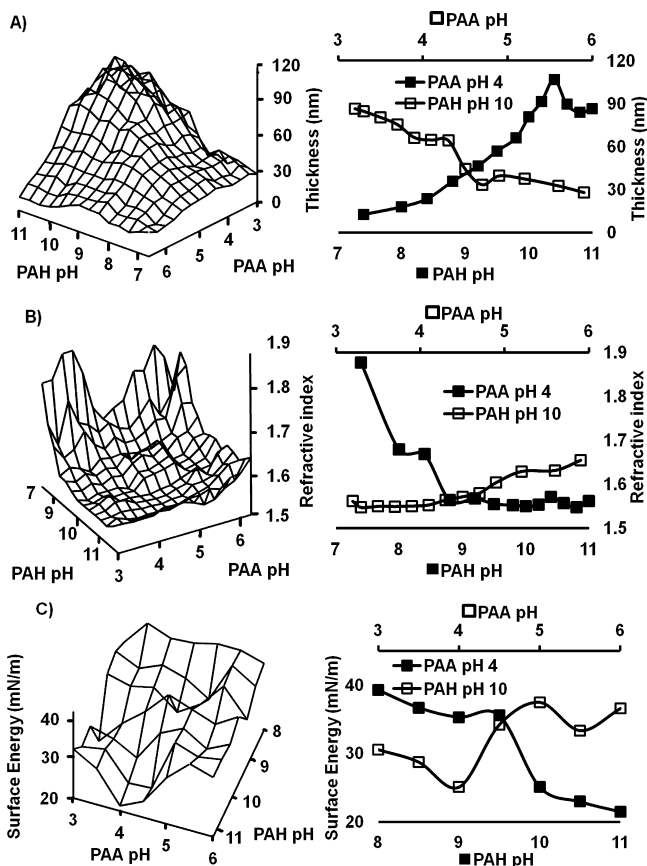


Figure 6. A 2D pH combinatorial dry (PAH/PAA)₅ film characterized with a (A) dry thickness map, (B) refractive index map, and (C) surface energy map.

uncertainties in independently measuring h and n as the limits of the ellipsometer are approached in ultrathin films.

The surface energy of the PEM film was then determined using sessile drop contact angles with both H₂O and CH₂I₂ (Figure 6C). Because of inherent nonhomogeneity of the gradients generated leading to asymmetric drops, averages of the left and right contact angles were used to approximate an average contact angle over a specific area of the film (~0.8 mm), and these were converted to surface energies using the Fowkes method (eq 1). In order to calculate the total surface energy, the total surface tension between the droplet and the air (γ_i), consisting of a polar component (γ_i^p) and a dispersive component (γ_i^d), was considered. Similarly, when the droplet was placed on a surface, a new interface was generated that had a total surface energy consisting of a polar (γ_s^p) and dispersive (γ_s^d) surface tension. Since CH₂I₂ does not have a polar component ($\gamma_s^p = 0$), γ_s^d can be directly calculated from CH₂I₂ contact angles and used with the H₂O contact angles to calculate γ_s^p .

$$\gamma_i(1 + \cos \theta) = 2(\sqrt{\gamma_i^p \gamma_s^p} + \sqrt{\gamma_i^d \gamma_s^d}) \quad (1)$$

At assembly PAH pH of ~10.5 and PAA pH of ~3.5 the total surface energy was calculated to be ~23 mN/m ($\gamma_s^d \approx 18$ mN/m and $\gamma_s^p \approx 5$ mN/m) while at assembly PAH pH of ~8 and PAA pH of ~6 the total surface energy was calculated to be ~42 mN/m ($\gamma_s^d \approx 41$ mN/m and $\gamma_s^p \approx 1$ mN/m). Interestingly, water contact angles were relatively high on all areas of the film (~90°) despite the composition of the film consisting of mainly polar groups. It is likely that when these

films were left to equilibrate in the atmosphere for several days, more water remained inside of the films than outside.²⁴ Since it is thermodynamically favorable for the -COOH groups to orient themselves toward the more polar medium (water polarity > air polarity), and since the mobility of the polyelectrolytes inside of the film is high, these groups could be effectively hidden inside of the film. It is plausible, then, that the -COOH groups settle into a thermodynamic minimum by forming dimers through hydrogen bonding, inhibiting remigration to the surface when submerged again (e.g., when placing a drop of water on the film). This would explain the large dispersive component of these films, since the water droplet would mostly be interacting with the hydrophobic carbon polymer backbone.²⁵

It was observed that the thicker, low-density film areas generally had a larger polar component to their surface energies than high-density films. It may be that due to a larger amount of loops and tails extruding from the surface in low-density film areas, polar group remained exposed to the surface, which is less likely with high-density PEM areas. Interestingly, the total surface energies on low-density PEM film areas were ~50% that of PEM areas of higher density (Figure 6C). Since low-density films are highly extrinsically charge-compensated, repulsion occurs between the long loops and tails, which would reduce adhesive interactions and thus possibly reduce total surface energy. Conversely, high-density films are highly intrinsically charge-compensated, resulting in increased adhesive interactions and thus potentially higher total surface energy.

c. Step Gradient Films. Step gradient films were generated by creating a pH gradient of one polyelectrolyte along the y -axis, while varying the number of bilayers along the x -axis while holding pH of the other polyelectrolyte constant. Films generated were at PAA pH 10 and PAH pH 10.5–3 (Figure 7A), PAH pH 3 and PAA pH 2.5–10 (Figure 7B), PAA pH 3 and PAH pH 10.5–3 (Figure 7C), and PAA pH 4.5 and PAH pH 10.5–3 (Figure 7D). When PAA was held at a pH of 10 (~100% ionization), no discernible film was formed (Figure 7A). At this pH, adsorbed PAA chains lack loops and tails, so the only significant surface loading was from PAH adsorption. However, at pH 10, previously adsorbed PAH chains have a

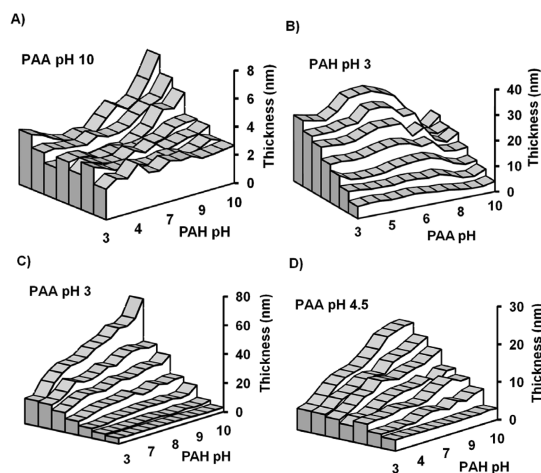


Figure 7. Step gradient films of thicknesses at different layer numbers for PAA and PAH. The pH of (A) PAA was fixed at pH 10.0, (B) PAH fixed at pH 4.5, (C) PAA fixed at pH 3.0, and (D) PAA fixed at pH 4.5. Six different bilayers were deposited in increasing order from the blank—the column closest to the axis.

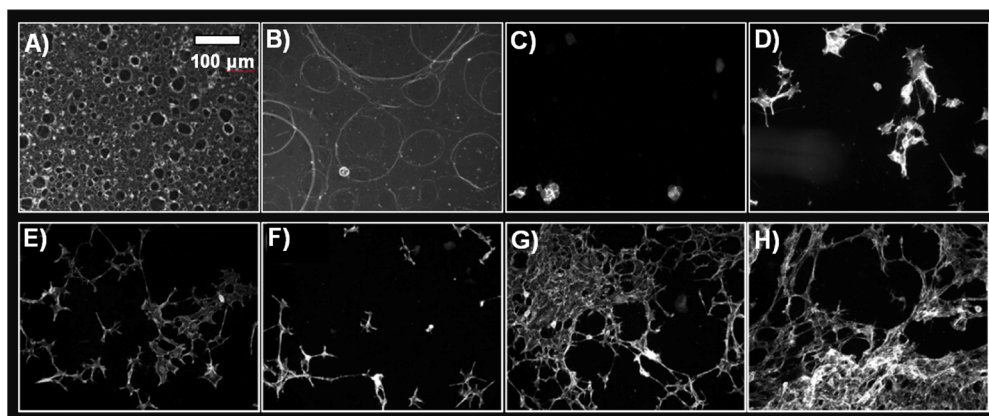


Figure 8. HEK 293 cells stained for actin filaments plated for 48 h in serum on PEM step gradient films represented in Figures 7B,C. Individual images correspond to (A) PAA pH 3, PAH pH 10.5 at 6 bilayers, (B) PAA pH 3, PAH pH 8 at 6 bilayers, (C) PAA pH 3, PAH pH 7 at 1 bilayer, (D) blank silicon wafer, (E) PAA pH 4.5, PAH pH 9 at 6 bilayers, (F) PAA pH 4.5, PAH pH 9 at 2 bilayers, (G) PAA pH 4.5, PAH pH 4 at 6 bilayers, and (H) PAA pH 4.5, PAH pH 4 at 2 bilayers.

low charge ratio, resulting in high interpenetration of PAA chains and little to no charge reversal of the surface. Thus, subsequent PAH chains will likely interact more with $-\text{NH}_2$ than $-\text{COO}^-$, preventing further adsorption.⁷

When PAA was varied from pH 2.5–10 and the pH of PAH was held constant at pH 3, an unusual sequence of thickness gradients is generated (Figure 7B). Considering only the degree of ionization of the individual polyelectrolytes, results found in Figure 7B should be similar to results found in Figure 7A, but they are not. It is possible that at low pHs, even though previously adsorbed PAA chains exhibit low charge, they also have strong hydrogen bond ordering (i.e., dimer formation), making interpenetration of the PAH energetically unfavorable due to the required breakage of this bond ordering. Lack of significant interpenetration would result in successful charge reversal of the surface and thus successful multilayer formation. This is unlike the situation depicted in Figure 7A, since amine hydrogen bond formation is much weaker and so allows more interpenetration of the layers, resulting in a lack of charge reversal at the surface and preventing multilayer formation. Furthermore, a reduction in film thickness at low PAA pHs suggests partial inhibition of diffusion by the previously adsorbed PAH terminal layer due to an increased surface charge density and resulting electrostatic charge barrier.²¹ Similar results have been observed by Shiratori et al. on individual films done at similar pH combinations⁷ and so were not investigated any further.

When PAA is held at a low pH (i.e., low charge density; Figure 7C), PAH assembly pH change seems to have little effect on thickness for the first 2–3 bilayers. This is due to incomplete surface coverage, which results in large interpenetration of the complementary PAH layer.²⁶ As was found by Fujita et al.,²⁷ total surface coverage seems to occur after three bilayers, and a continuous thickness increase is subsequently observed with increasing PAH assembly pH. If the pH of PAA is held at 4.5 (Figure 7B), a drastic decrease in overall film thickness is observed compared to films made when PAA is held at pH 3 (Figure 7C). At high charge densities, the amount of loops is minimal, leading to lower surface loading,²⁸ lower initial thickness, and higher surface coverage. The higher surface coverage reduces subsequent interpenetration, and thus the effect of PAH assembly pH change is immediately discernible, unlike in the film depicted in Figure 7C.

HEK 293 Cell Viability. HEK 293 cells were plated on step gradient films with thickness profiles depicted in Figures 7C,D. Film bilayer step gradients built at a constant PAA pH of 4.5 (Figure 7D) were completely biocompatible. Greatest viability occurred on thinner areas of the films, such as those built at a PAH assembly pH of 4; for example, Figures 8G and 8H depict cells grown on a 6 bilayer area and a 2 bilayer area of the film, respectively. Reduced viability was observed on thicker regions of the film, such as those built at a PAH assembly pH of 10.5; for example, Figures 8E and 8F depict cells grown on a 6 bilayer area and a 2 bilayer area of the film, respectively. Alternatively, step gradient films built at a constant PAA assembly pH of 3 (Figure 7C) were completely cell resistant at all PAH assembly pHs, irrespective of the number of bilayers (Figures 8A–C); cell survival only occurred on the blank area of the film (Figure 8D; coated *in situ* by serum proteins). Interestingly, as little as one bilayer made under these conditions was enough to make the surface completely resistant to cells (Figure 8C). Overall, the results suggest that although cell viability is strongly dependent on assembly conditions, it is largely independent of the number of layers deposited on the surface.

As a comprehensive test on both axes at once, HEK 293 cells were plated on full 2D combinatorial films (Figure 9) and were observed to be most viable (cell nuclei counts after 48 h) at intermediate regimes of pH fabrication conditions. These optimal growth conditions were discovered not at the extremes of fabrication pH, but instead near PAH pHs of 4–6 and PAA

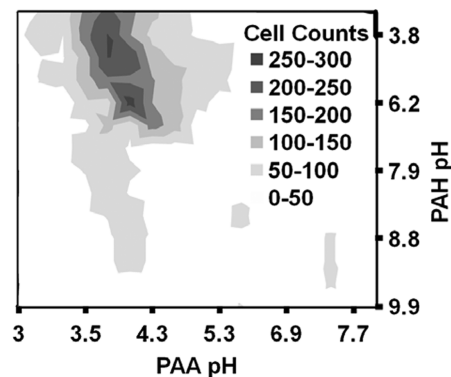


Figure 9. HEK 293 cell viability on a (PAA/PAH)₅ combinatorial film.

pH around 4. This cell viability “phase plot” clearly illustrates selectivity of HEK 293 cells on PAA/PAH fabrication pH conditions and suitability of this combinatorial method for optimizing cellular screening.

Considering just the films fabricated at pH 10.5, 9, 7, and 5, with measured modulus values of 170, 120, 1800, and 6500 kPa, respectively;¹⁷ then the degree of cell viability follows a general trend predicting that HEK 293 cells grow better on substrates with a higher modulus (Figure 10). Indeed, there

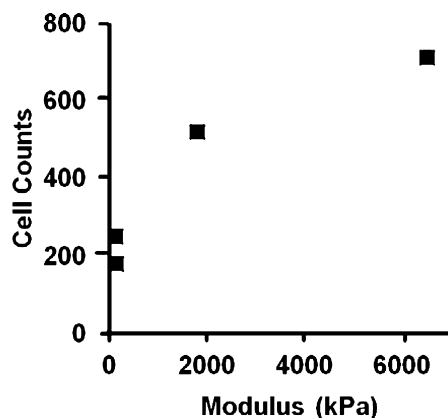


Figure 10. Relationship between PEM modulus and HEK 293 cell viability.

seems to be a growing consensus that cellular behavior is highly dependent on the modulus of a material.^{9,29–38} A more full study of cell response to modulus is currently underway, but there appears enough data here to suggest that film stiffness plays an important role in tailoring cell behavior.

CONCLUSIONS

A new PEM fabrication technique was developed that enabled the production of a variety of widely tunable 2D PEM gradient and step gradient films. Via this new technique, it is now possible to make just one PEM film out of PAA and PAH that represents all of the usual possible stable pH and salt assembly conditions, essentially recreating all of the usual thousands of individual PAA/PAH films on one combinatorial silicon wafer. Using these PEM combinatorial films, it was observed that assembly conditions had a strong effect on cell viability. Additionally, PEM bilayer step gradient films demonstrated that the number of layers had relatively little effect on cell viability and that one bilayer built with PAA at pH 3 was enough to make the film completely resistant to cells. In conjunction with the development of many automatic characterization techniques, the development of new combinatorial methods such as this in PEM film production could aid significantly the optimization of conditions for various biotechnological applications by reducing this enormous parameter space into one sample by reducing costs and increasing precision and accuracy. The device designed here is a manual prototype to serve as a proof of concept, but one could easily envisage that newer versions of the device could be completely automated.

AUTHOR INFORMATION

Corresponding Author

*E-mail: Christopher.Barrett@mcgill.ca

Notes

The authors declare no competing financial interest.

ACKNOWLEDGMENTS

The authors thank NSERC Canada and CIHR Canada for financial support through a CREATE Team Training Grant in Neuro Engineering. The authors are grateful to K. Lai Wing Sun and T. Kennedy of the Montreal Neurological Institute for assistance with the cell measurements and helpful discussions on interpretation.

REFERENCES

- (1) Decher, G.; Schmitt, J. In *Trends in Colloid and Interface Science VI*; Helm, C., Lösche, M., Möhwald, H., Eds.; Springer: Berlin, 1992; Vol. 89, pp 160–164.
- (2) Decher, G. *Science* **1997**, *277*, 1232–1237.
- (3) Hiller, J. A.; Mendelsohn, J. D.; Rubner, M. F. *Nat. Mater.* **2002**, *1*, 59–63.
- (4) Dorris, A. C.; Douglas, K. L.; Tabrizian, M.; Barrett, C. J. *Can. J. Chem.* **2008**, *86*, 1085–1094.
- (5) Schüler, C.; Caruso, F. *Biomacromolecules* **2001**, *2*, 921–926.
- (6) Mendelsohn, J. D.; Yang, S. Y.; Hiller, J. A.; Hochbaum, A. L.; Rubner, M. F. *Biomacromolecules* **2002**, *4*, 96–106.
- (7) Shiratori, S. S.; Rubner, M. F. *Macromolecules* **2000**, *33*, 4213–4219.
- (8) Fasolka, M. J.; Amis, E. J. *Combinatorial Materials Science: Measures of Success*; John Wiley & Sons, Inc.: New York, 2006; p 1.
- (9) Brocchini, S.; James, K.; Tangpasuthadol, V.; Kohn, J. J. *Biomed. Mater. Res.* **1998**, *42*, 66–75.
- (10) Gravert, D. J.; Datta, A.; Wentworth, P.; Janda, K. D. *J. Am. Chem. Soc.* **1998**, *120*, 9481–9495.
- (11) Takeuchi, T.; Fukuma, D.; Matsui, J. *Anal. Chem.* **1998**, *71*, 285–290.
- (12) Meredith, J. C.; Sormana, J. L.; Keselowsky, B. G.; García, A. J.; Tona, A.; Karim, A.; Amis, E. J. *J. Biomed. Mater. Res., Part A* **2003**, *66A*, 483–490.
- (13) Kennedy, S. B.; Washburn, N. R.; Simon, J. C. G.; Amis, E. J. *Biomaterials* **2006**, *27*, 3817–3824.
- (14) Tomlinson, M. R.; Efimenko, K.; Genzer, J. *Macromolecules* **2006**, *39*, 9049–9056.
- (15) Tomlinson, M. R.; Genzer, J. *Macromolecules* **2003**, *36*, 3449–3451.
- (16) Xu, C.; Wu, T.; Mei, Y.; Drain, C. M.; Batteas, J. D.; Beers, K. L. *Langmuir* **2005**, *21*, 11136–11140.
- (17) Mermut, O.; Lefebvre, J.; Gray, D. G.; Barrett, C. J. *Macromolecules* **2003**, *36*, 8819–8824.
- (18) Fowkes, F. M. *Ind. Eng. Chem.* **1964**, *56*, 40–52.
- (19) Schlenoff, J. B.; Li, M. *Ber. Bunsenges. Phys. Chem.* **1996**, *100*, 943–947.
- (20) Mermut, O.; Barrett, C. J. *J. Phys. Chem. B* **2003**, *107*, 2525–2530.
- (21) Lavalle, P.; Picart, C.; Mutterer, J.; Gergely, C.; Reiss, H.; Voegel, J.-C.; Senger, B.; Schaaf, P. *J. Phys. Chem. B* **2003**, *108*, 635–648.
- (22) Dubas, S. T.; Schlenoff, J. B. *Macromolecules* **1999**, *32*, 8153–8160.
- (23) Tanchak, O. M.; Barrett, C. J. *Chem. Mater.* **2004**, *16*, 2734–2739.
- (24) Tanchak, O. M.; Yager, K. G.; Fritzsche, H.; Harroun, T.; Katsaras, J.; Barrett, C. J. *Langmuir* **2006**, *22*, 5137–5143.
- (25) Yasuda, T.; Okuno, T.; Yasuda, H. *Langmuir* **1994**, *10*, 2435–2439.
- (26) Ladam, G.; Schaad, P.; Voegel, J. C.; Schaaf, P.; Decher, G.; Cuisinier, F. *Langmuir* **1999**, *16*, 1249–1255.
- (27) Fujita, S.; Shiratori, S. *Nanotechnology* **2005**, *16*, 1821.
- (28) Schach, R.; Hommel, H.; Van Damme, H.; Dejardin, P.; Amsterdamsky, C. *Langmuir* **2004**, *20*, 3173–3179.
- (29) Mehrotra, S.; Hunley, S. C.; Pawelec, K. M.; Zhang, L.; Lee, I.; Baek, S.; Chan, C. *Langmuir* **2010**, *26*, 12794–12802.
- (30) Larkin, A. L.; Davis, R. M.; Rajagopalan, P. *Biomacromolecules* **2010**, *2788–2796*.

- (31) Thompson, M. T.; Berg, M. C.; Tobias, I. S.; Lichter, J. A.; Rubner, M. F.; Van Vliet, K. J. *Biomacromolecules* **2006**, *7*, 1990–1995.
- (32) Schneider, A.; Francius, G.; Obeid, R.; Schwinté, P.; Hemmerlé, J.; Frisch, B.; Schaaf, P.; Voegel, J.-C.; Senger, B.; Picart, C. *Langmuir* **2005**, *22*, 1193–1200.
- (33) Gray, D. S.; Tien, J.; Chen, C. S. *J. Biomed. Mater. Res., Part A* **2003**, *66A*, 605–614.
- (34) Yeung, T.; Georges, P. C.; Flanagan, L. A.; Marg, B.; Ortiz, M.; Funaki, M.; Zahir, N.; Ming, W.; Weaver, V.; Janmey, P. A. *Cell Motil. Cytoskeleton* **2005**, *60*, 24–34.
- (35) Discher, D. E.; Janmey, P.; Wang, Y.-l. *Science* **2005**, *310*, 1139–1143.
- (36) Ren, K.; Crouzier, T.; Roy, C.; Picart, C. *Adv. Funct. Mater.* **2008**, *18*, 1378–1389.
- (37) Lichter, J. A.; Thompson, M. T.; Delgadillo, M.; Nishikawa, T.; Rubner, M. F.; Van Vliet, K. J. *Biomacromolecules* **2008**, *9*, 1571–1578.
- (38) Huang, J.; Peng, X.; Xiong, C.; Fang, J. J. *Colloid Interface Sci.* **2011**, *355*, 503–508.